Effects of Bizelesin (U-77779), a Bifunctional Alkylating Minor Groove Agent, on Genomic and Simian Virus 40 DNA†

Jan M. Woynarowski,‡,§ Mary M. McHugh,‡ Loretta S. Gawron,‡ and Terry A. Beerman*,‡

Department of Experimental Therapeutics, Roswell Park Cancer Institute, Elm and Carlton Streets, Buffalo, New York 14263, and Cancer Therapy and Research Center, Institute for Drug Development, 14960 Omicron Drive, San Antonio, Texas 78245

Received June 15, 1995⊗

ABSTRACT: Bizelesin is a bifunctional covalent minor groove binding agent which forms adducts with 3′-adenines on opposite DNA strands. DNA lesions induced by bizelesin in genomic DNA of BSC-1 cells, as well as intracellular and purified simian virus 40 (SV40) DNA, were examined. Alkaline sucrose sedimentation analysis indicated a nonrandom distribution of heat-labile damage in BSC-1 cell genomic DNA with frequencies of 1−60 lesions/10^6 base pairs (bp) for bizelesin concentrations from 10 to 400 nM, respectively. Extrapolation of these data suggested that, at 0.15 nM bizelesin, ~10^2 adducts per cell may be sufficient to inhibit cell growth by 90% (D_{10}). While the frequency of bizelesin adducts in intracellular SV40 DNA was comparable to that in genomic DNA, higher levels of lesion formation are observed with purified SV40 DNA. Chromatin structure has little effect on localization of bizelesin adducts since treatment of either infected cells or purified SV40 DNA reveals a similar pattern of drug-induced damage. Bizelesin adduction sites (mapped on the SV40 genome as thermally-induced strand breaks at 50−100 bp resolution) are found in regions centered at 4200, 3900, 4700, and ~5200. The location of these regions of intense bizelesin bonding coincides with the sites of potential cross-links predicted using the 5′-T-(A/T)$_4$-A-3′ sequence. The analysis of bizelesin adducts at the sequence level in the 3943−4451 SV40 DNA fragment indicated that 40% of total damage was in potential cross-linking sites and an additional 35% in the 5′-A-(A/T)$_4$-A-3′ monoalkylating sites. Bizelesin-induced interstrand cross-links have been demonstrated directly in the 3943−4451 SV40 DNA fragment by alkaline electrophoresis.

Bizelesin (Figure 1) is a cyclopropylpyrroloindole (CPI) DNA alkylating agent (Mitchell et al., 1991) derived from the natural compound CC-1065 by modification in the B subunit (for review, see Warpehoski, 1991, and Reynolds et al., 1986). This alteration appears to be responsible for elimination of the delayed toxicity that disqualified CC-1065 as a clinical drug candidate (Li & Krueger, 1991; Warpehoski, 1991). Many CPI drugs are unusually potent antiproliferative agents, and several (including bizelesin) are being considered for clinical trials (Li et al., 1991).

The interaction of CPI agents with purified DNA, characterized elsewhere (Boger et al., 1991a,b; Hurley et al., 1991; Lee & Gibson, 1993; Reynolds et al., 1985; Sun & Hurley, 1993), has certain unique features. CPI agents form noncovalent complexes with AT-rich DNA sequences in the minor groove by means of hydrophobic interactions and van der Waals forces. In contrast, sequence recognition by classical minor groove binders, such as distamycin, involves formation of specific hydrogen bonds (Lown, 1992). Once bound to the minor groove in a noncovalent fashion, CPI drugs are capable of alkylating the N3 position of adenine residues at the 3′ end of the binding sites. CC-1065 with a single cyclopropyl group is capable of only monofunctional alkylation (Reynolds et al., 1986; Warpehoski, 1991). In contrast, bizelesin, a tail to tail dimer of a monofunctional CPI, features two chloromethyl groups capable of covalently bonding two 3′ terminal adenine residues in the complementary strands (Mitchell et al., 1991). The resulting interstrand cross-links are responsible for more stringent sequence requirements for drug bonding compared to monofunctional CPI bonding (Ding et al., 1993; Lee & Gibson, 1993; Lee et al., 1994; Sun & Hurley, 1993).

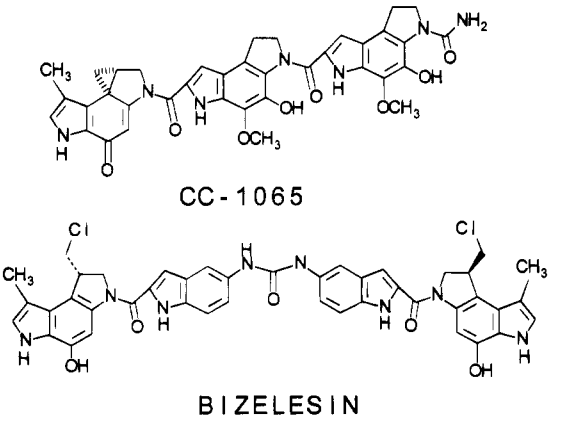

FIGURE 1: The structures of CC-1065 and bizelesin.

Previous studies demonstrated an ability of CC-1065 and certain other monofunctional CPI agents to induce covalent DNA adducts in intact cells (McHugh et al., 1994; Bhuyan et al., 1992; Tang et al., 1994; Weiland & Dooley, 1991; Zsido et al., 1992, 1991). While bizelesin is more cytotoxic than CC-1065, lesions in cellular DNA were detected only at bizelesin concentrations that produced more than a three-

† This study was supported in part by grants from the American Cancer Society (DHP-133) and the National Cancer Institute (CA 16056) to T.A.B. and by CTRC Research Foundation, San Antonio, TX, to J.M.W.

* To whom correspondence should be addressed.
‡ Roswell Park Cancer Institute.
§ Institute for Drug Development.

⊗ Abstract published in *Advance ACS Abstracts,* September 15, 1995.

0006-2960/95/0434-13042$09.00/0

log cell kill (Lee & Gibson, 1991). Thus, the importance of bizelesin adducts for antiproliferative activity remains unclear. In this study, we quantitated bizelesin adducts formed in BSC-1 cells and examined their relationship to cell growth inhibition. In addition to genomic DNA, we assessed bizelesin lesions on a defined DNA target, SV40 DNA.

EXPERIMENTAL PROCEDURES

Drugs and Chemicals. Bizelesin and CC-1065, generously provided by Dr. Patrick McGovren at the Upjohn Co. (Kalamazoo, MI), were dissolved in dimethylacetamide (Aldrich Chemical, Milwaukee, WI) and stored at −20 °C protected from light.

Cell Cultures and SV40 Infection. BSC-1 African green monkey kidney cells were cultured as described previously (Zsido et al., 1991). When drug effects on intracellular SV40 DNA were examined, BSC-1 cells were infected with the virus at 5−15 plaque forming units per 6×10^5 cells (in 35 mm dishes) as described previously (Grimwade et al., 1988). Cells were treated with drug 40 h after infection.

BSC-1 Cell Survival. Survival of bizelesin-treated uninfected cells was determined by colony formation as described previously (Zsido et al., 1991). Briefly, following drug treatment, cells were washed with phosphate-buffered saline (PBS), trypsinized, and plated at various cell concentrations. After 8−10 days incubation at 37 °C, the colonies were stained with methylene blue and counted. The results are expressed as relative plating efficiency (i.e., the mean plating efficiency relative to control plates).

Bizelesin-Induced Heat-Labile Sites in Genomic BSC-1 Cell DNA. Covalent bizelesin adducts in genomic DNA were quantitated by induction of heat-labile sites (Zsido et al., 1991). Briefly, drug-treated [^{14}C]thymidine-radiolabeled cells were mixed with untreated [^{3}H]thymidine-radiolabeled cells (internal controls) and heated for 15 min at 90 °C in 1% sarkosyl, 1 M NaCl, and 10 mM EDTA, pH 8.6. Lysates (equivalent to $(0.15-0.2) \times 10^6$ cells) were loaded on 5−30% alkaline sucrose gradients overlaid with a lysing layer (0.3 mL of 1% sarkosyl in 2.5% sucrose in gradient buffer). Samples were centrifuged at 12 000 rpm for 20 h in an SW41Ti rotor, followed by fractionation from the top, and the radioactivity per fraction was determined by scintillation counting. The radioactivity in each gradient fraction was converted to dpm and expressed as a percent of the total recovered radioactivity. Sedimentation coefficients ($s_{20,w}$) and molecular weights for each fraction were estimated according to Young and Krumlauf (1981) and Studier (1965), respectively. The slope of the linear portion of the gradient was 4.4 S/fraction. Peak deconvolution was achieved by fitting actual sedimentation data to a number of overlapping Gaussian distribution profiles using a template in Microsoft Excel. The fit was optimized using the least squares method and Excel Solver to calculate peak positions, standard deviations, and weighting factors for underlying Gaussian components. The sum of resulting Gaussian components coincided with the actual profiles. (The Excel template for peak deconvolution is available by request from J.M.W.)

Adduct Frequencies in Uninfected BSC-1 Cell Genomic DNA. Frequencies of heat-labile sites (breaks) in genomic DNA were calculated as described previously (Zsido et al., 1991) from the equation:

$$f = \frac{((MW_n)_A/(MW_n)_B) - 1}{(MW_n)_A/640} \quad (1)$$

where f is the number of breaks per base pair and $(MW_n)_A$ and $(MW_n)_B$ are the number average molecular weights of the [^{3}H]- and [^{14}C]-radiolabeled DNA peaks, respectively. The value 640 represents the average molecular weight of one DNA base pair. The number average molecular weight was determined using the equation:

$$(MW_n) = \frac{\sum \%R_i}{\sum \%R_i/MW_i} \quad (2)$$

where $\%R_i$ is percent of recovered radioactivity for each fraction of a given peak and MW_i is the molecular weight of the corresponding fraction. When adduct frequencies were expressed per cell, DNA content was assumed to be 8.7 μg/10^6 cells (McHugh et al., 1995).

Bizelesin Damage to Intracellular and Purified SV40 DNA Measured by Topological Forms Conversion. Drug treatment of SV40 infected cells and subsequent purification of viral DNA as well as drug treatment of purified SV40 DNA (Gibco BRL, Grand Island, NY, 0.8 μg/0.4 mL) were performed as described earlier (McHugh et al., 1994). Briefly, 40 h after infection, plates were rinsed once with PBS and incubated for 30 min with fresh medium prior to drug treatment. Purified SV40 DNA (800 ng) was incubated in 0.4 mL of TE [10 mM Tris-HCl, pH 7.6, 1 mM ethylenediaminetetraacetic acid (EDTA)]. All incubations with bizelesin were for 4 h at 37 °C with the indicated drug concentrations. Reactions were terminated by adjustment to a final concentration of 1% sodium dodecyl sulfate (SDS), and intracellular samples were digested for an additional 2 h with proteinase K (50 μg/mL). All DNA samples were then extracted with phenol/chloroform/isoamyl alcohol (25:24:1) to remove unbound bizelesin and heated for 2 h at 75 °C to convert drug adducts to strand breaks. After heating, topological forms were separated by agarose gel electrophoresis. Following Southern transfer and autoradiography, the amount of DNA in individual forms was quantitated using a laser densitometer (Molecular Dynamics). Frequencies of heat-labile sites in SV40 DNA were estimated based upon Poisson distribution of the conversion of form I SV40 DNA to form II SV40 using the equation:

$$f = \frac{-\ln(FI)}{L} \quad (3)$$

where f is the number of breaks per base pair, FI represents fraction of nonadducted (remaining) form I of SV40 DNA, and L is the length of SV40 DNA (5243 bp).

Localization of Bizelesin-Induced Heat-Labile Sites in the SV40 Genome. Adduct distribution (i.e., heat-labile damage) along the SV40 genome was examined by restriction enzyme digestion analysis as described previously for CC-1065 (McHugh et al., 1994). Drug-treated intracellular and purified SV40 DNA was prepared as described for the topological forms conversions assay and subjected to digestion with *Eco*RI nuclease, agarose gel electrophoresis, Southern blotting and hybridization, autoradiography, and quantitation on a laser densitometer. The migration distance was plotted against the logarithm of the length of marker

fragments in order to determine the fragment length of each band. The length of DNA fragments was used to determine the distance of the bizelesin-induced break from the unique enzyme restriction site.

Distribution of Potential Bizelesin Cross-Linking Sites in SV40 DNA. The prevailing type of cross-linking site for bizelesin was defined as 5′-T-(A/T)$_4$-A*-3′, where 3′-adenines on each strand are alkylated by the drug (Sun & Hurley, 1993). For each position in the SV40 sequence (strain 776, GenBank), we determined the number of possible orientations conforming to the preferred bonding sequence ("hit" probability). To pinpoint regions with high intensity sites as well as with clusters of lower intensity sites, the data were smoothed by calculating moving averages of hit probabilities at each nucleotide position (averaged over a window of ±10 bp) using the equation:

$$D(N_i) = \frac{\sum_{i-w}^{i+w} I(N)}{2w+1} \quad (4)$$

where $D(N_i)$ is the moving average of hit density at N_i nucleotide, $I(N)$ is hit probability, and w is window ($w = 10$ bp).

Sites of Bizelesin Adducts in the SV40 DNA Fragment (3943−4451). A singly end-radiolabeled 508 bp fragment of SV40 (from position 3943 to position 4451) was synthesized by polymerase chain reaction. The following 21-mer oligonucleotides were used as the forward and reverse primers, respectively: MAR-U (5′-TACATCCCAAGCAA-TAACAAC-3′) and MAR-L (5′-CTACTCCTCCAAAAAA-GAAGA-3′). The primers (HPLC purified) were obtained from Genosys (The Woodlands, TX). Either one of the primers was end-radiolabeled with [γ-^{32}P]ATP using T4 polynucleotide kinase (New England Nuclear Biolabs) according to the manufacturer's protocol. Labeled primers were purified on Sephadex G-25 Quick Spin columns (Boehringer-Mannheim, Indianapolis, IN) followed by ethanol precipitation. Polymerase chain reactions (50 μL) consisted of 10 pg of SV40 DNA, one labeled and one unlabeled primer (0.5 μM each), 1 unit of Taq polymerase, 1.5 mM $MgCl_2$, and 0.2 mM of each deoxynucleotide triphosphate, in 1× Taq polymerase buffer II (all reagents from AmpliTaq PCR kit, Perkin-Elmer, Norwalk, CT). Thermocycling was performed in a Model 9600 thermal cycler (Perkin-Elmer). The following conditions were used: 95 °C for 30 s, followed by 30 cycles of: 35 °C for 20 s, 72 °C for 45 s, and 94 °C for 15 s. The final cycle was followed by an extra 4 min of extension at 72 °C. [^{32}P]-end-radiolabeled PCR product was purified on a Sephadex G-100 or Sepharose CL-6B Quick Spin column (Boehringer Mannheim, Indianapolis, IN). An aliquot of the reaction was analyzed on an agarose gel along with Mass Markers (Gibco-BRL, Grand Island, NY) to provide an estimate of product yield. The (3943−4451) fragment (250 ng) labeled either at the 5′ end of the top strand or at the 5′ end of the bottom strand was treated with bizelesin at 2 and 10 μM in 16 μL of TE buffer supplemented with 100 mM NaCl for 4 h at 37 °C followed by ethanol precipitation. Samples were dissolved in 10 μL of TE buffer and heated at 95 °C for 15 min to convert adducts to strand breaks. Heated samples were mixed with 4 μL of sequencing loading buffer (95% formamide, 0.05% bromophenol blue, 0.05% xylene blue, and 20 mM EDTA). Aliquots from each sample (2.5 μL) were analyzed by electrophoresis in 8% polyacrylamide/8.3 M urea sequencing gel. The sequencing reactions for the top and bottom strands of the (3943−4451) fragment were generated with Sequenase version 2 (USB, Cleveland, OH) by dideoxy method using the same MAR-U and MAR-L primers and Sequenase manufacturer's protocol.

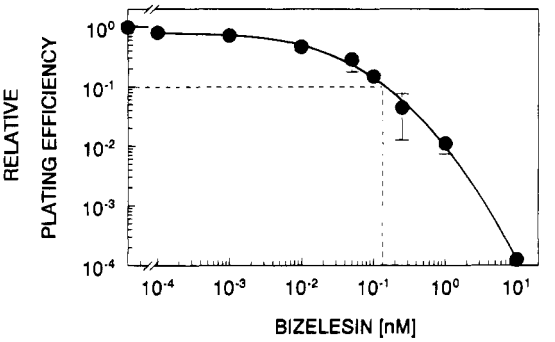

FIGURE 2: Inhibition of survival of BSC-1 cells treated with bizelesin for 4 h. Following drug treatment, cell monolayers were washed with PBS, trypsinized, and replated. Relative plating efficiency was measured by colony formation.

Formation of Interstrand Cross-Links in an SV40 DNA Fragment. A singly end-radiolabeled 508 bp fragment of SV40 (from position 3943 to position 4451) was synthesized by polymerase chain reaction as described above. Approximately 2 μg of labeled DNA (6 × 10^4 cpm) was treated with bizelesin in 40 μL for 4 h at 37 °C. DNA was precipitated with ethanol to remove unreacted drug, redissolved in TE buffer, and analyzed by alkaline agarose electrophoresis (Sambrook et al., 1989). The positions of unlabeled size markers (stained with ethidium bromide) were used to calculate the sizes of radiolabeled bands.

RESULTS

Inhibition of Survival of BSC-1 Cells. The ability of BSC-1 cells to form colonies was examined after a 4 h treatment with bizelesin under the conditions used to assess drug effects on cellular DNA. Such conditions revealed a potent effect of bizelesin with 90% inhibition of plating efficiency (D_{10}) observed at approximately 0.15 nM (Figure 2). In comparison, the D_{10} for continuous incubation of plated cells with bizelesin was 0.02 nM (data not shown).

Bizelesin-Induced Heat-Labile Sites in Genomic BSC-1 Cell DNA. A characteristic property of CC-1065, as well as bizelesin adducts in DNA is their ability to undergo thermal elimination accompanied by breakage of the phosphate backbone (Ding & Hurley, 1991; Hurley et al., 1991; Reynolds et al., 1985). In this study, we assayed bizelesin generation of such heat-labile sites by alkaline sucrose gradient sedimentation (Zsido et al., 1991). In the assay, drug-treated [^{14}C]thymidine-radiolabeled cells are mixed with untreated [^{3}H]thymidine-radiolabeled cells before lysis and heating. The use of [^{3}H]-radiolabeled cells as internal controls facilitates the detection and quantitation of low levels of drug-induced damage.

Identical sedimentation profiles were observed for both [^{14}C]- and [^{3}H]thymidine-radiolabeled untreated cells (Figure 3A). The induction of heat-labile sites resulted in a shift in the sedimentation profile of bizelesin-treated samples toward

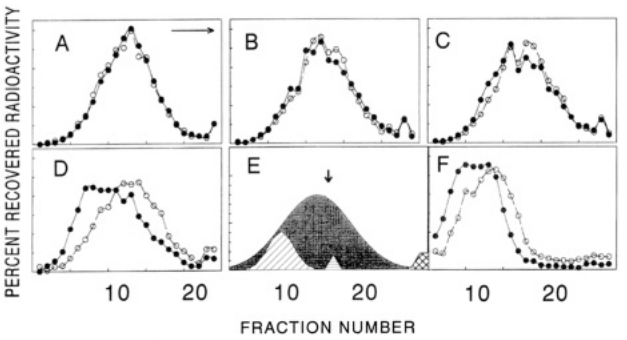

FIGURE 3: Bizelesin-induced heat-labile sites in genomic BSC-1 cell DNA. [^{14}C]Thymidine-radiolabeled BSC-1 cells were treated for 4 h with bizelesin. Cell suspensions were mixed with untreated [^{3}H]thymidine-radiolabeled cells (internal controls), lysed, heated, and analyzed by sedimentation on alkaline sucrose gradients. Panels A−D correspond to cells treated with bizelesin at the following concentrations: 0 nM (A), 50 nM (B), 100 nM (C), and 400 nM (D). Panel E shows deconvolution of the [^{14}C] profile of cells treated with 400 nM bizelesin from panel D into two main components peaking at fractions 7 and 11 (see Experimental Procedures for details). Panel F shows the sedimentation profile of DNA from cells treated with 100 nM CC-1065. The symbols in panels A−D and F correspond to drug-treated [^{14}C]thymidine-radiolabeled DNA samples (●) and to untreated [^{3}H]thymidine-radiolabeled cells (○).

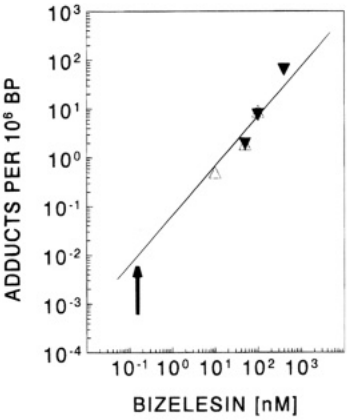

FIGURE 4: Frequency of bizelesin adducts in uninfected BSC-1 cells. Adduct formation was detected as heat-labile sites based on sedimentation analysis after 4 h drug treatment. Adduct frequencies were calculated as described in Experimental Procedures. The results are expressed as the number of adducts per 10^6 base pairs (BP). Different symbols represent independent experiments. The arrow indicates the D_{10} value (drug concentration that inhibited cell survival by 90%) from Figure 2.

the top of the gradients. Little effect was observed for bizelesin at 50 or 100 nM (Figure 3B,C). The effect of 400 nM drug was more pronounced, resulting in a broad band of degraded [^{14}C]-radiolabeled DNA (Figure 3D). The shape of this band suggested the presence of more than one component. Deconvolution of the [^{14}C]sedimentation profile from panel D revealed two main peaks at fractions 7 and 11 (Figure 3E). Deconvolutions of the [^{3}H] profile (internal control for 400 nM bizelesin) as well as profiles for external controls resulted in a single peak at approximately 50 S (data not shown). This observation suggested that bizelesin-induced damage was not randomly distributed in cellular DNA.

Under the same conditions, higher levels of thermally-induced damage are observed with CC-1065. For example, the effect of CC-1065 at 100 nM (Figure 3F) was similar to that of bizelesin at 400 nM. Moreover, consistent with our previous findings (Zsido et al., 1991), CC-1065 treatment also caused a shift in the profile of the [^{3}H]thymidine-radiolabeled internal control. Such a shift probably reflects the presence of small amounts of unreacted drug in the lysates which are available for interaction with the control DNA. In contrast, sedimentation of the internal controls for bizelesin-treated samples was unaltered, suggesting that much of the bizelesin in lysates from drug-treated cells was unavailable for reaction with control DNA, probably because of formation of covalent adducts.

To provide a quantitative assessment of drug-induced damage to BSC-1 cell genomic DNA, we estimated lesion frequencies based on the shape and positions of the respective sedimentation profiles. Figure 4 shows the results plotted as the number of adducts per 10^6 base pairs (bp). Thermally induced damage with 10 nM bizelesin was minimal, effecting a lesion frequency of less than 1 adduct/10^6 bp. The highest drug level (400 nM) induced 63 heat-labile sites/10^6 bp. Quantitation of the deconvoluted components of the sedimentation profile for 400 nM drug (see Figure 3E) resulted in 124 and 51 adducts/10^6 bp for a smaller and larger peak, respectively. Given the ratio of the smaller to larger peak, it appears that approximately one-third of the adducts are localized in 15% of the total DNA.

The low frequency of bizelesin adducts prevents their detection at drug levels that result in limited inhibition of cell growth. The lowest drug levels that produce any detectable lesions correspond to 4 logarithms of cell kill. However, the order of magnitude of lesion frequency at drug levels below the limits of detectability can be estimated by extrapolating the data in Figure 4. If the extrapolation is linear, it would predict roughly one lesion per 10^8 bp at a bizelesin concentration equal to the drug's D_{10} (0.15 nM).

Quantitation of Bizelesin Damage to Intracellular and Purified SV40 DNA. To further characterize bizelesin lesions in intracellular DNA, we examined drug effects on intracellular SV40 DNA. Overall damage to SV40 DNA was assessed based on the thermally-induced conversion of topological forms. Figure 5A illustrates the distribution of SV40 DNA forms after intracellular treatment with bizelesin followed by heating for 2 h at 75 °C. These conditions, resulting in induction of bizelesin strand breaks in SV40 DNA comparable to that obtained after heating at 90 °C for 15 min, prevented artifactual changes in supercoiled form I which were observed in control (no drug) samples heated at the higher (90 °C) temperature (data not shown). After heating, DNA adducted with bizelesin shows a concentration-dependent decrease in the proportion of form I and concomitant increase in forms II (nicked) and III (linear) SV40 DNA (see lanes 1−4, 0−10 μM bizelesin, respectively). Panels B and C show bizelesin-induced topological forms conversion in intracellular and purified SV40 DNA, respectively, quantitated from a series of experiments. Increases in both single- (form II) and double-strand (form III) damage are observed when infected cells are treated with ≥1.0 μM bizelesin. A similar profile of single- and double-strand damage was observed with purified DNA, albeit at lower concentrations. A 50% conversion of form I is observed with 0.05 or 2 μM bizelesin treatment of purified or intracellular SV40 DNA, respectively.

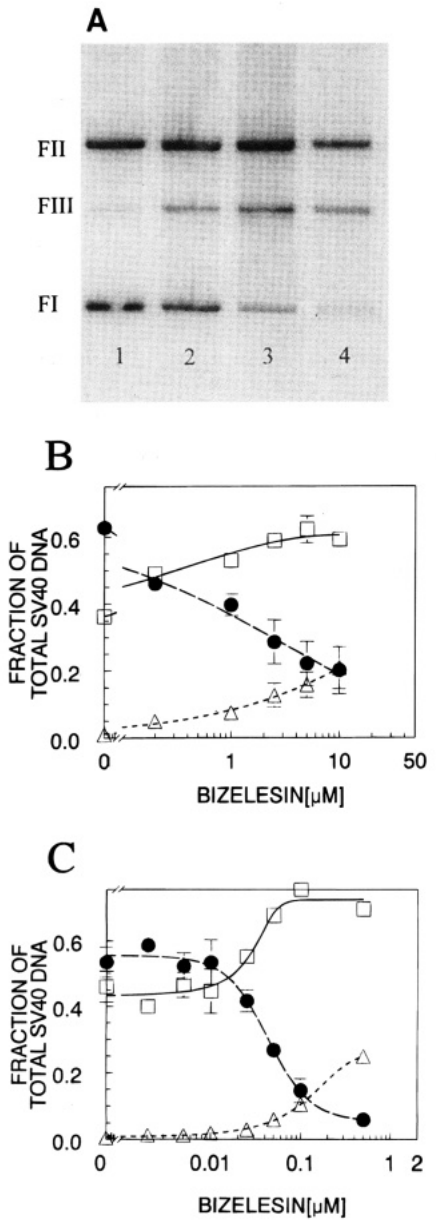

FIGURE 5: Bizelesin damage to intracellular and purified SV40 DNA measured by topological forms conversion. Samples were heated for 2 h at 75 °C to convert drug adducts to breaks before electrophoresis in agarose gels. Gels were subjected to Southern blotting and probed with the *Eco*RI−*Bam* H1 fragment of SV40 DNA. Panel A is an autoradiogram of a representative agarose gel after electrophoresis of SV40 DNA from BSC-1 cells incubated with bizelesin at 0 μM (lane 1), 0.2 μM (lane 2), 2.5 μM (lane 3), and 10 μM (lane 4). Positions of supercoiled DNA (FI), nicked (FII), and linear (FIII) are indicated. Panels B and C show the quantitation of heat-labile bizelesin-induced damage in intracellular and purified SV40 DNA, respectively, based on densitometry of the autoradiograms. Relative amounts of topological forms [FI (●), FII (□), and FIII (△)] are expressed as a fraction of the total SV40 DNA. Points represent mean values ± SEM from 3 experiments. For purified DNA treated with 0.1 μM bizelesin, the initial drug/DNA ratio corresponded to 1 drug molecule/31 bp.

To relate drug damage in SV40 DNA to that in genomic DNA, we estimated the frequencies of bizelesin-induced adducts in SV40 DNA based on the decrease in form I. With intracellular treatment of SV40 DNA, lesion frequencies are 59 breaks/10^6 bp and 88 breaks/10^6 bp at 0.2 and 1 μM bizelesin, respectively. These values are similar to the 63 breaks/10^6 bp observed in genomic DNA at 0.4 μM bizelesin (Figure 4). By contrast, when purified SV40 is treated with 0.5 μM drug, a higher frequency of lesions (i.e., 435 breaks/10^6 bp) is observed, resulting in a 90% conversion of form I DNA (see Figure 5).

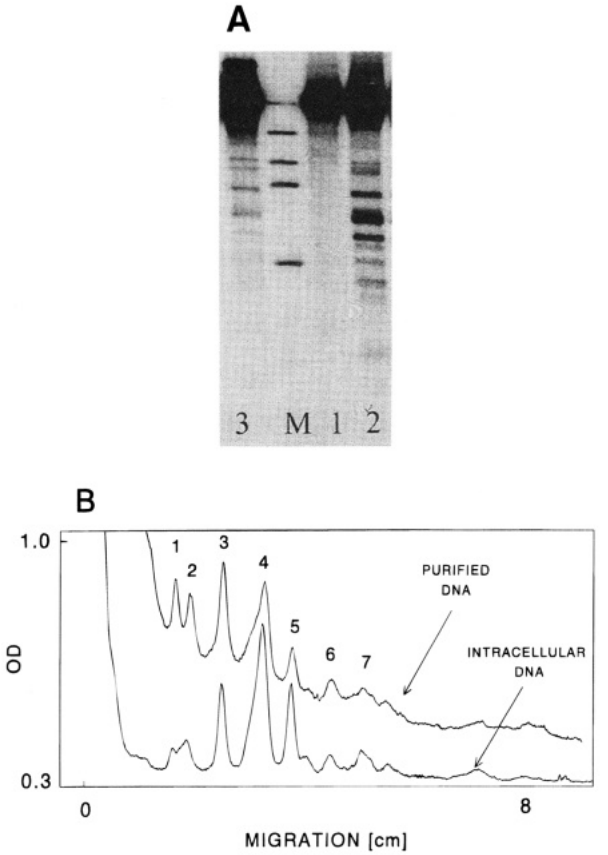

FIGURE 6: Localization of bizelesin-induced heat-labile sites in the SV40 genome. DNA was treated with bizelesin for 4 h and then heated for 2 h at 75 °C to convert drug adducts to breaks. Following digestion with *Eco*RI nuclease, which cuts at a single site on the SV40 genome, samples were electrophoresed on agarose gels, subjected to Southern blotting, and probed with the [^{32}P]-radiolabeled *Eco*RI−*Bam*H1 fragment of SV40 DNA. Panel A: Autoradiogram showing SV40 DNA from infected cells incubated with 0 μM (lane 1) or 2.5 μM (lane 2) bizelesin. Lane 3 shows purified SV40 DNA incubated with 50 nM bizelesin. Positions of SV40 DNA size markers are indicated (M). Panel B shows densitometric profiles of lanes containing purified SV40 DNA treated with 50 nM bizelesin or DNA from infected cells treated with 0.25 μM bizelesin. Peak positions corresponding to the location of double-strand break sites were determined by comparison to migration of the DNA size marker, while the relative density of each point on the graph was calculated as a fraction of total density of the lane. The arrows indicate the position of double-strand breaks at about (1) 100, (2) 5100, (3) 4700, (4) 4200, and (5) 3900 on the SV40 genomic map. Several bands of lower intensity (e.g., around 2600, 3400, 3600) also were observed. The intense form III band is shown at 0 migration. The values for the relative intensity of purified DNA were offset by 0.2 to allow both intracellular and purified DNA profiles to be shown on the same graph.

Localization of Bizelesin-Induced Heat-Labile Sites in the SV40 Genome. Having demonstrated the ability of bizelesin to induce heat-labile intracellular SV40 DNA damage, we examined the distribution of drug adducts along the SV40 genome. Strand damage induced by heat treatment of bizelesin-adducted SV40 DNA was assessed after restriction with *Eco*RI nuclease and agarose gel electrophoresis. An autoradiogram obtained after electrophoresis and Southern blotting of selected lanes from a gel containing bizelesin-treated intracellular or cell-free SV40 DNA is shown in Figure 6A. One band corresponding to full-length SV40

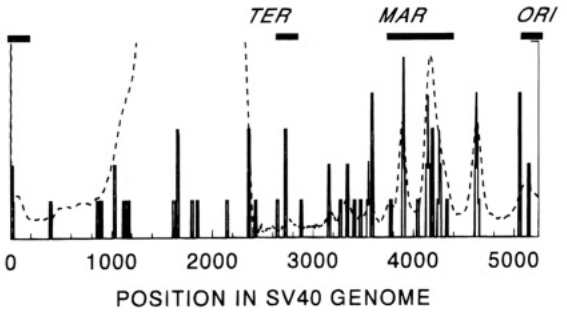

FIGURE 7: Predicted distribution of high affinity bizelesin binding sites on the SV40 sequence. The solid lines show hit probabilities at each nucleotide position for the 68 potential preferred sites of bizelesin cross-links (5′-T-(A/T)$_4$-A-3′) with 42 nonoverlapping positions. The broken line shows the actual densitometric profile for heated bizelesin-adducted intracellular SV40 DNA from Figure 6B. This profile was aligned to the position scale using the average position of the largest peak (approximately 4200 bp). Because the gel could not resolve DNA fragments with molecular weights close to that of form III (5243 base pairs), the positions between 600 and 2300 could not be mapped using *Eco*RI restriction.

DNA was apparent in DNA from untreated infected cells (lane 1), as well as from untreated purified SV40 DNA (data not shown). When infected cells were treated with 2.5 μM bizelesin, thermally-induced breaks resulted in three main and several minor bands (lane 2). A similar pattern of DNA damage was nioted when purified SV40 DNA was treated with 50 nM bizelesin (lane 3).

To facilitate localization of bizelesin-adducted sites on the SV40 genome, the densitometric profiles of agarose gel lanes containing DNA from infected cells treated with 0.25 μM bizelesin or purified SV40 DNA treated with 50 nM bizelesin were aligned (see Figure 6B). Bizelesin treatment of either purified or intracellular SV40 DNA produces similar patterns of heat-labile damage, although some differences in relative intensity are observed. For both treatment systems, much of the damage is localized to at least three regions: around 3900, 4200, and 4700. Other sites also are observed around 100, 2600, 3400, 3600, and 5100. The bizelesin concentrations in this figure were shown in Figure 5 to effect 50% conversion of intracellular or purified SV40 from I DNA.

Predicted vs Actual Sites of Bizelesin Adducts. The localization of bizelesin DNA damage might be explained by a nonuniform distribution of the drug's consensus sequences throughout the SV40 genome. While bizelesin has been shown to bond to a variety of sequences, especially at higher drug/DNA ratios, the preferred sequence where 3′-adenines on each strand can be alkylated is 5′-T-(A/T)$_4$-A*-3′ (potential cross-linking sites; Sun & Hurley, 1993). Since this consensus sequence was found by analyzing short linear DNA fragments, its validity for much larger supercoiled DNA was not certain. Analysis of the SV40 sequence indicated that SV40 DNA contains 68 potential preferred sites for bizelesin cross-links. These sites may be occupied maximally by 42 adducts in nonoverlapping orientations. The distribution of these potential sites (with their predicted intensities) is shown in Figure 7. Comparison with the tracing of the actual densitometric scan of intracellular DNA taken from Figure 6B reveals a good coincidence between the predicted and actual sites. The regions as well as the relative band intensities appear similar. For example, even the low intensity sites have counterparts in the predicted adducts. A portion of the SV40 genome (3600−4400) has been identified as the site of association with the nuclear matrix (Pommier et al., 1990) and is one of the regions where bizelesin sites, both predicted and actual, are found.

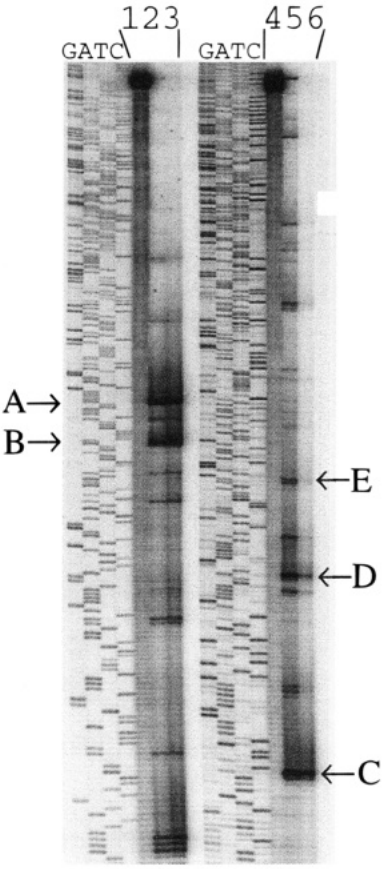

FIGURE 8: Bizelesin adducts in the 3943−4450 fragment of SV40 DNA. The figure shows the representative polyacrylamide sequencing gel showing thermally-induced subfragments that reflect breaks at the sites of bizelesin adducts (see Experimental Procedures for details). Lanes 1 and 4 reprsent control fragments with top and bottom strand, respectively, 5′ end-labeled with ^{32}P. Lanes 2 and 3 correspond to the fragments incubated with bizelesin at 2 or 10 μM, respectively. Lanes denoted G, A, T, and C contain respective sequencing reactions with the same primer as used to label the (3943−4450) fragment. The indicated intense bands correspond to the adducts at the following positions: 4156 (A), 4140 and 4141 (B), 4333 (C), 4292 (D), and 4265 and 4266 (E). The initial drug/DNA ratio (at 2 μM bizelesin) corresponded to 1 drug molecule/12 bp.

Bizelesin Adducts in the SV40 DNA Fragment (3943−4451). The region of the SV40 genome that was shown by low resolution mapping to be highly damaged by bizelesin was used to map precise positions of drug adducts. These experiments used the 508 bp fragment (3943−4451) that was uniquely 5′ end-labeled with ^{32}P in either the top or the bottom strand. The positions of adducted bases were determined based on thermally-induced breaks (Sun & Hurley, 1993). The results confirm the sequence specificity of bizelesin adducts. The polyacrylamide sequencing gel in Figure 8 shows some of the most intense sites on both strands of the (3943−4451) fragment (marked A−E). The sequences corresponding to these and other sites of relative intensities greater than 0.5% are listed in Table 1. With three exceptions, these sites indicated bizelesin bonding to adenine. Sites at positions 4290 and 4380 suggested G alkylation, while one site at 4365 suggested T alkylation. Infrequent bizelesin alkylations at G or T have been observed previously (Sun & Hurley, 1993).

Table 1: Bizelesin Adducts in the SV40 DNA Fragment (3943−4450)

Position	Relative Intensity[a] %	5′	6	5	4	3	2	1	0	-1	3′
Top Strand											
4156	15.3[b]		C	A	A	A	T	T	A	A	
4157	15.3[b]		A	A	A	T	T	A	A	A	
4140	9.1		C	T	T	A	T	T	A	A	
4141	8.7		T	T	A	T	T	A	A	C	
4158	6.8		A	A	T	T	A	A	A	A	
4160	6.8		T	T	A	A	A	A	A	G	
4049	6.6		G	A	T	T	A	A	A	A	
4048	4.8		G	G	A	T	T	A	A	A	
4023	4.6		T	T	G	T	T	T	A	G	
4047	4.4		G	G	A	A	T	T	A	A	
4149	4.3		C	C	C	T	T	T	A	C	
4090	2.1		T	C	A	A	T	A	A	C	
4063	1.6		T	C	C	T	T	T	A	A	
4089	1.6		C	T	C	A	A	T	A	A	
4121	1.5		C	A	C	T	A	T	A	C	
4130	1.3		T	C	A	A	A	T	A	T	
4194	1.2		T	T	A	T	T	A	A	T	
4232	1.1		G	A	A	A	A	A	A	C	
4097	1		C	A	G	A	A	A	A	T	
4123	0.8		C	T	A	T	A	C	A	T	
4197	0.6		A	T	T	A	A	T	A	G	
Bottom Strand											
Position	**Relative Intensity[a] %**	**5′**	**6**	**5**	**4**	**3**	**2**	**1**	**0**	**-1**	**3′**
4333	38.2		C	T	A	T	T	T	A	C	
4292	20.3		A	A	A	A	T	T	A	T	
4282	4.1		A	A	A	A	A	T	A	T	
4296	3.5		C	A	A	G	A	A	A	A	
4318	3.5		G	G	A	A	A	A	A	G	
4317	3.1		A	G	G	A	A	A	A	A	
4358	2.3		A	G	T	A	A	T	A	G	
4360	2.2		T	T	A	G	T	A	A	T	
4364	2.2		G	T	G	T	T	T	A	G	
4361	2.0		T	T	T	A	G	T	A	A	
4189	1.9		T	T	A	A	T	A	A	C	
4266	1.9		T	T	T	A	T	A	A	G	
4265	1.8		C	T	T	T	A	T	A	A	
4290	1.8		A	A	T	T	A	T	G	G	
4285	1.4		T	G	G	A	A	A	A	A	
4135	1.0		T	T	A	A	T	A	A	G	
4192	0.9		C	T	A	T	T	A	A	T	
4380	0.9		T	T	T	T	T	T	G	A	
4365	0.7		T	G	T	G	T	T	T	A	
4379	0.7		T	T	T	T	T	G	A	G	
4303	0.6		T	G	C	T	A	T	A	C	
4246	0.5		G	T	T	A	T	A	A	T	
4045	0.5[c]		A	T	T	T	T	A	A	T	
4046	0.5[c]		G	A	T	T	T	T	A	A	

[a] Relative intensities were calculated for each strand separately. The positions and relative intensities of the sites on the top and bottom strands are shown. Position "0" denotes the adducted bases at the 3′ end of drug binding sites. Bands of intensity lower than 0.5% were omitted from the table. [b] The value represents half of the sum for the sites 4156 and 4157 that were quantitated as one band. [c] The value represents half of the sum for the sites 4045 and 4046 that were quantitated as one band.

The relative intensities of various sites for adenine adducts varied depending on whether the top or bottom strand was analyzed. For the top strand, approximately 70% of the signal intensity was found at seven sites. For the bottom strand, the three most intense sites accounted for over 60% of the signal intensity. After normalization for both strands together, 40% and 35% of the total damage was observed at sequences 5′-T-(A/T)$_4$-A*-3′ and 5′-A-(A/T)$_4$-A*-3′, respectively. The former sequence corresponds to potential interstrand cross-links and the latter to the sites for monofunctional adduct formation (Sun & Hurley, 1993). An additional 25% of the total intensity corresponded to adducts at 5′-NNN-(A/T)$_2$-A*-3′, where the NNN triplet contained either one or two G or C, preferably at positions closer to the 5′ end.

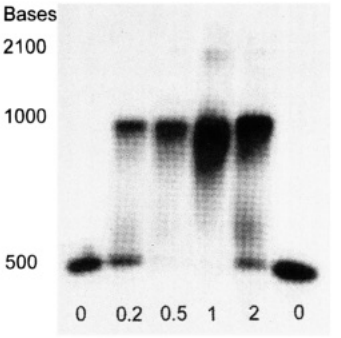

FIGURE 9: Bizelesin cross-link formation in the 3943−4450 fragment of SV40 DNA. A singly end-radiolabeled SV40 DNA fragment (508 bp) was obtained by polymerase chain reaction. Following bizelesin treatment, the [^{32}P]-radiolabeled fragment was electrophoresed on an alkaline agarose gel. The arrows indicate the size of the DNA fragments determined from the migration of DNA size markers. At 0.2 μM bizelesin, the initial drug/DNA ratio corresponded to 1 drug molecule/400 bp.

Formation of Interstrand Cross-Links in the SV40 DNA Fragment (3943−4451). The sequences of adducted sites suggested that bizelesin could form interstrand cross-links in several locations between 3943 and 4451. The induction of cross-links in this region of SV40 DNA was reexamined using the 508 bp SV40 fragment (3943−4451) and alkaline agarose gel electrophoresis (Figure 9). Under alkaline strand separating conditions, untreated DNA migrated the distance determined for a 500 nucleotide marker. Bizelesin treatment resulted in alterations in mobility of the fragment. At 0.2 μM bizelesin (estimated ratio of 1 drug per 400 bp), a new band appeared which migrated the distance expected for a DNA fragment twice the size of the control fragment. This band probably represents cross-linked DNA for which complete strand separation is not possible. Assuming a Poisson distribution, 0.2 μM bizelesin produced one cross-link per 500 bp. At 0.5−1 μM bizelesin, cross-linking reached saturation. At 2 μM bizelesin, the 500 nucleotide band reappeared, possibly as a result of excessive formation of monoadducts in orientations not suitable for cross-linking. The origin of an additional band of roughly 2100 bases (at 1 μM bizelesin) remains unknown. Figure 9 shows data for the radiolabeled forward primer, but similar results were obtained with the [^{32}P]-radiolabeled reverse primer (data not shown). This experiment confirms that bizelesin readily reacts with and forms cross-links in this region of SV40 genome.

DISCUSSION

Many DNA-reactive agents induce large numbers of nonspecific DNA lesions throughout the entire genome. For example, cisplatinum analogs require more than 1.2×10^6 lesions per cell to inhibit cell growth by 90% (Ploy et al., 1984). In contrast, bizelesin, a cyclopropylpyrroloindole bifunctional AT-specific alkylating agent, induces infrequent lesions in cellular DNA (Lee & Gibson, 1991). Our observations using sedimentation analysis to detect and quantitate heat-labile sites are consistent with a low level of bizelesin adduct formation. By extrapolating the adduct frequency data, a 90% reduction in cell growth is observed

with 10^2 bizelesin lesions per cell, compared to $\sim 10^4$ lesions per cell induced by the parent drug, CC-1065. Thus, lesions induced by bizelesin are 100 times more cytotoxic than those induced by CC-1065.

Localization of bizelesin adducts in specific regions of the genome may be a factor in bizelesin cytotoxicity. Since sedimentation analysis suggested the presence of differentially affected subpopulations of cellular DNA, bizelesin lesions on genomic DNA may indeed be nonrandomly distributed. Whether localized regions of DNA in intact cells could be targeted by bizelesin was examined using intracellular SV40 DNA. Mapping of adducts by restriction enzyme digestion analysis of SV40 DNA from bizelesin-treated cells indicated that drug bonding sites were limited. Similar to uninfected cells, bizelesin damage to intracellular SV40 DNA was limited to fewer sites than that observed for CC-1065 (McHugh et al., 1994), although similar regions of the SV40 genome were affected by both CPI drugs. Much of the drug-induced damage was observed in three regions (around 3900, 4200, and 4700) which correspond to sites for topoisomerase II cleavage located in or near the SV40 matrix-associated region (MAR, 3610−4377; Pommier et al., 1990). An additional region around 5200 is within the SV40 origin of replication (Campbell, 1986).

At the level of sequence analysis, the bizelesin study showed good agreement between the observed regions of intense damage and the adduction sites predicted using 5′-T-(A/T)$_4$-A-3′, one of the possible sequences for formation of interstrand cross-links (Sun & Hurley, 1993). The actual sites of bizelesin adduction were determined in the 3943−4451 SV40 fragment, where low resolution mapping (i.e., restriction enzyme digestion analysis) showed some of the most intense damage. The analysis indicated that 40% of total damage was in potential cross-linking sites 5′-T-(A/T)$_4$-A-3′ and an additional 35% in monoalkylating sites 5′-A-(A/T)$_4$-A-3′. While additional sequences have been described as sites for bizelesin adduction in purified DNA (Ding & Hurley, 1991; Lee & Gibson, 1993; Sun & Hurley, 1993), the significance of such sites in intact cells is unknown. It is possible that different cell lines, DNA targets, or methodologies for lesion detection may reveal different localizations of bizelesin adducts, such as those found by Lee et al. (1994) in the p53 gene of human colon carcinoma.

Although differences in the intensity of bizelesin adduct formation in certain regions were noted, similar regions of the genome were damaged in both intracellular and purified SV40 DNA systems. Thus, the chromatin structure of intracellular SV40 DNA does not alter the localization of bizelesin bonding (within 50−100 bp resolution). However, drug concentrations needed to produce damage in purified SV40 DNA are lower than in infected cells. Likewise, differences in damage efficiency between purified and intracellular SV40 DNA have been observed for CC-1065 (McHugh et al., 1994), as well as for DNA strand scission drugs, such as C-1027, neocarzinostatin, and macromomycin (McHugh et al., 1995; Grimwade & Beerman, 1986). This reduced lesion formation in whole cells suggests limited entry of bizelesin into the cell.

As with CC-1065 (Zsido et al., 1991), bizelesin lesions were not readily reversible upon postincubation in drug-free medium (data not shown). Since CPI−DNA adducts are not bulky lesions and induce minimal changes in DNA structure (Ding & Hurley, 1991), it is possible that CPI adducts are poor substrates for excision-repair enzymes. However, bizelesin differs from monofunctional CPI analogs in the length of time required for formation of DNA adducts. Maximal induction of heat-labile bizelesin lesions in intact cells was observed only after 3 h incubation (data not shown) compared to 1 h required for induction of heat-labile sites induced by monofunctional analogs such as CC-1065 or adozelesin. This difference may reflect an ability of bifunctional bizelesin, but not monofunctional CPI's, to induce cross-links in intracellular DNA. Interstrand DNA cross-links have been reported elsewhere to be an important component of bizelesin interaction with purified DNA (Sun & Hurley, 1993), and a long time course of lesion formation is consistent with the slow kinetics of the bizelesin second arm reaction observed in purified DNA (Lee & Gibson, 1991). Recently, we quantitated bizelesin-induced interstrand cross-links in BSC-1 cells using sedimentation in alkaline sucrose gradients of unheated cellular DNA (Woynarowski and Napier, unpublished). The frequencies of interstrand cross-links are similar to those of heat-labile sites (reported here). For example, bizelesin induced approximately 0.8 and 5 cross-links per 10^6 bp at 10 and 100 nM, respectively.

Our results indicate that bizelesin bonds to specific regions of intracellular DNA. Bizelesin adducts are relatively infrequent compared to other DNA-reactive drugs. Such infrequent DNA lesions, possibly interstrand cross-links, appear to be highly cytotoxic. In SV40 DNA, bizelesin adducts are observed in functionally important AT-rich regions of the genome. Consistent with such damage, bizelesin is a potent inhibitor of BSC-1 genomic and SV40 DNA replication (Woynarowski and Beerman, unpublished). Further studies will examine the mechanism by which bizelesin bonding affects DNA replication.

ACKNOWLEDGMENT

The authors would like to thank Steve Kotsopoulos and William Chapman for excellent technical assistance.

REFERENCES

Berezney, R. (1991) *J. Cell. Biochem. 47*, 109−123.
Bhuyan, B. K., Smith, K. S., Adams, E. G., Petzold, G. L., & McGovren, J. P. (1992) *Cancer Res. 52*, 5687−5692.
Boger, D. L., Munk, S. A., & Zarrinmayeh, H. (1991a) *J. Am. Chem. Soc. 113*, 3980−3983.
Boger, D. L., Munk, S. A., Zarrinmayeh, H., Ishizaki, T., Haught, J., & Bina, M. (1991b) *Tetrahedron 47*, 2661−2682.
Boulikas, T. (1993) *J. Cell. Biochem. 52*, 14−22.
Bubley, G. J., Teicher, B. A., Ogata, G. K., Sandoval, L. S., & Kusumoto, T. (1994a) *Biochem. Pharmacol. 48*, 145−153.
Bubley, G. J., Ogata, G. K., Dupuis, N. P., & Teicher, B. A. (1994b) *Cancer Res. 54*, 6325−6329.
Ding, Z. M., & Hurley, L. H. (1991) *Anti-Cancer Drug Des. 6*, 427−452.
Ding, Z. M., Harshey, R. M., & Hurley, L. H. (1993) *Nucleic Acids Res. 21*, 4281−4287.
Grimwade, J., & Beerman, T. (1986) *Mol. Pharmacol. 30*, 358−363.
Grimwade, J. E., Cason, E. B., & Beerman, T. A. (1988) *Biochim. Biophys. Acta 950*, 102−112.
Hurley, L. H., Warpehoski, M. A., Lee, C.-S., McGovren, J. P., Scahill, T. A., Kelly, R. C., Mitchell, M. A., Wicnienski, N. A., Gebhard, I., Jihnson, P. D., & Bradford, V. S. (1991) *J. Am. Chem. Soc. 112*, 4633−4649.
Lee, C.-S., & Gibson, N. W. (1991) *Cancer Res. 51*, 6586−6591.
Lee, C. S., & Gibson, N. W. (1993) *Biochemistry 32*, 9108−9114.
Lee, C. S., Pfeifer, G. P., & Gibson, N. W. (1994) *Biochemistry 33*, 6024−6030.

Li, L. H., & Krueger, W. C. (1991) *Pharmacol. Ther. 51*, 239–255.

Li, L. H., Swenson, D. H., Schpok, S. L., Kuentzel, S. L., Dayton, B. D., & Krueger, W. C. (1982) *Cancer Res. 42*, 999–1004.

Li, L. H., Kelly, R. C., Warpehoski, M. A., McGovren, J. P., Gebhard, I., & DeKoning, T. F. (1991) *Invest. New Drugs 9*, 137–148.

Lown, J. W. (1992) *Antiviral Res. 17*, 179–196.

McHugh, M. M., Woynarowski, J. M., Mitchell, M. A., Gawron, L. S., Weiland, K. L., & Beerman, T. A. I. P. B. (1994) *Biochemistry 33*, 9158–9168.

McHugh, M. M., Woynarowski, J. M., Gawron, L. S., Otani, T., & Beerman, T. A. (1995) *Biochemistry 34*, 1805–1814.

Mitchell, M. A., Kelly, R. C., Wicnienski, N. A., Hatzenbuhler, N. T., Williams, M. G., Petzold, G. L., Slightom, J. L., & Siemienak, D. R. (1991) *J. Am. Chem. Soc. 113*, 8894–8895.

Ploy, A. C. M., van Dijk, M., & Lhman, P. H. M. (1984) *Cancer Res. 44*, 2043–2051.

Pommier, Y., Cockerill, P. N., Kohn, K. W., & Garrard, W. T. (1990) *Virology 64*, 419–423.

Reynolds, V. L., Molineux, I. J., Kaplan, D. J., Swenson, D. H., & Hurley, L. H. (1985) *Biochemistry 24*, 6228–6237.

Reynolds, V. L., McGovren, J. P., & Hurley, L. H. (1986) *J. Antibiot. 39*, 319–334.

Sambrook, J., Fritsch, E. F., & Maniatis, T. (1989) *Molecular Cloning. A Laboratory Manual* (Nolan, C., Ed.) 2nd ed., p 6.20, Cold Spring Harbor Laboratory Press, Plainview, NY.

Studier, F. W. (1965) *J. Mol. Biol. 11*, 373–390.

Sun, D., & Hurley, L. H. (1993) *J. Am. Chem. Soc. 115*, 5925–5933.

Tang, M., Qian M., & Pao, A. (1994) *Biochemistry 33*, 2726–2732.

Warpehoski, M. (1991) *Drugs Future 16*, 131–141.

Weiland, K. L., & Dooley, T. P. (1991) *Biochemistry 30*, 7559–7568.

Young, B. D., & Krumlauf, R. (1981) *Anal. Biochem. 115*, 97–101.

Zsido, T. J., Woynarowski, J. M., Baker, R. M., Gawron, L. S., & Beerman, T. A. (1991) *Biochemistry 30*, 3733–3738.

Zsido, T. J., Beerman, T. A., Meegan, R. L., Woynarowski, J. M., & Baker, R. M. (1992) *Biochem. Pharmacol. 43*, 1817–1822.

BI951357W